DLCTLungDetectNet: Deep Learning for Lung Tumor Detection in CT scans

Ms. Seema B. Rathod *
Research Scholar Lokmanya Tilak College of Engineering
Navi Mumbai University, India
omseemarathod@gmail.com

Dr. Lata L. Ragha
Fr. C. Rodrigues Institute of Technology
Navi Mumbai University, India
lata.ragha@fcrit.ac.in

Abstract: Lung cancer is a critical global health concern, necessitating precise early diagnosis and intervention for better patient outcomes. Computed Tomography (CT) scans are pivotal in lung cancer detection, and leveraging advanced technology is crucial. This study introduces "DLCTLungDetectNet," a Convolutional Neural Network (CNN) based deep learning framework, with a focus on early lung cancer detection using CT scan images. The core innovation lies in the integration of the robust "FusionNet," a hybrid model amalgamating feature from ResNet50 and InceptionV3. We conduct a comprehensive comparative analysis, showcasing the superior performance of DLCTLungDetectNet over established architectures such as VGG16, VGG19, and Inception v3. Rigorous evaluation based on standard metrics substantiates DLCTLungDetectNet's high accuracy, precision, Area Under Curve (AUC), and F1 score. This research not only highlights the potential of deep learning in enhancing lung cancer diagnosis but also establishes a benchmark, showcasing the efficacy of the FusionNet hybrid model for achieving superior accuracy in automated lung tumor detection.

Keywords— Lung cancer, CT scan imaging, Deep Learning, CNN, FusionNet, VGG16, VGG19, Inception v3, ResNet50, Deep Learning.

1. Introduction

Lung cancer remains one of the most formidable and prevalent health challenges globally, significantly impacting public health and necessitating urgent, accurate diagnoses for effective treatment and improved patient outcomes(Manafi-Farid et al., 2022).Early detection and timely intervention are paramount in mitigating the mortality rates associated with lung cancer. In the realm of medical imaging, Computed Tomography (CT) scans have emerged as indispensable tools for lung cancer detection, offering high-resolution images that are crucial for precise diagnosis(Ozdemir et al., 2020). The intricate and nuanced patterns present in these images, however, demand sophisticated analytical approaches for accurate interpretation. In recent years, the integration of deep learning methodologies, particularly Convolutional Neural Networks (CNNs),(Chlap et al., 2021) has shown remarkable promise in automating the analysis of medical images and aiding healthcare professionals in accurate diagnostics. Deep Learning for Lung Tumor Detection in CT scans (DLCTLungDetectNet) presents a concerted effort to harness the potential of CNN-based deep learning frameworks specifically designed for early lung cancer detection using CT scan images. This study explores an innovative approach to feature extraction and classification, aiming to significantly enhance the accuracy and efficiency of lung tumor detection compared to traditional methods(Chlap et al., 2021). DLCTLungDetectNet's strength lies in its unique hybrid model, FusionNet, which expertly merges features extracted from ResNet50 and InceptionV3(Habuza et al., 2021). This fusion of influential pre-trained models enhances the network's ability to capture intricate patterns and complex features within the lung images, ultimately bolstering the accuracy of tumor detection(Kaulgud & Patil, 2023). The proposed framework undergoes thorough evaluation and comparison with other prominent deep learning architectures, namely VGG16, VGG19, and Inception v3, to validate its superior performance in terms of accuracy, precision, Area Under Curve (AUC), and F1 score.

This research not only underscores the potential of deep learning in revolutionizing lung cancer diagnostics but also emphasizes the significance of model fusion strategies for achieving superior accuracy in automated lung tumor detection(Saini et al., 2021). The subsequent sections delve into the methodology, dataset specifics, proposed CNN architecture, results, and discussions, providing comprehensive insights into DLCTLungDetectNet and its pivotal role in advancing the field of lung cancer detection using CT scan imaging(Mathews & Jeyakumar, 2020).

Various nations have evaluated systems for lung tumour detection, as the majority of people on Earth face the risk of this deadly cancer, leading to fatalities(Sakr, 2022). The NLST evaluation revealed that existing low-quality CT scan images were used, resulting in lower accuracy, and radiologists had to deal with a large number of CT scan images as a consequence of these procedures(Masood et al., 2020).[2]Due to the challenging nature of identifying lesions, even experienced physicians may find it difficult to visualize them. Consequently, the workload on radiologists significantly escalates when they have to analyse a larger number of CT images (Zhou et al., 2023). In this paper a total of 356 Jordanians was diagnosed with lung cancer, accounting for 7.7% of all newly reported cases. The ratio of male to female lung cancer cases was 5:1, with 297 (13.1%) men and 59 (2.5%) women. Among men, lung cancer ranked second in terms of the prevalence, while it ranked tenth among women(Pise & Rege, 2021).As breast, colon, and prostate cancers continue to increase, they contribute to a significant number of deaths(Sultana et al., 2021). Lung cancer alone accounts for approximately 170,000 excess deaths and 180,000 new cases annually, resulting in about 480 daily diagnoses and 460 deaths (Tina, 2005). The global climate and pollution have resulted in millions of lives lost and increased cancer cases. This poses a significant challenge in the 21st century, as stated by the World Health Organization (Kim & Lee, 2023)) After pre-processing, the focus of this discussion is on how segmentation and feature extraction assist in lung cancer diagnosis, including the description of feature categories and extraction methods.

2. Related Work

Traditional image processing techniques are employed to enhance image quality in this research (Sharma et al., 2023) To ensure accurate diagnoses, improving the quality of medical images is essential. This research employs the highly effective Discrete Wavelet Transform method for noise removal in the images. (Phelan et al., 2023) In this research, the authors used the Wiener and median filters in pre-processing. The filters were compared using the PSNR parameter, and the results demonstrated that the Wiener filter outperformed the median filter, yielding superior results (Huang et al., 2022). In this research, the median, bilateral, and discrete cosine transformation techniques were used to remove noise from images. EEG data was utilized as input for the study. (Firdaus et al., 2020) The objective of this study is to generate high-quality images using nonlinear filtering algorithms. Evaluation is based on parameters such as PSNR, MSE, SNR, and MAE.(Nuhic & Kevric, 2020) In all the research, various filters are employed for pre-processing and improving the image quality. These include Wavelet Transform, NL-means filters, multiple filters such as average, Gaussian, log, median, and Wiener filters, as well as the Gaussian filter(Chen et al., 2021).Implemented in this method are image processing and machine learning approaches for predicting and distinguishing between tumour and non-tumour forms based on CT scan images(Muto et al., 2023). Evaluation parameters include geometrical, statistical, and gravy-level characteristics. The system achieves an accuracy of 84%, sensitivity of 97.14%, and specificity of 53.33%(Ladjal et al., 2021). Nevertheless, the accuracy of tumour detection is deemed unsatisfactory, and the absence of machine learning methods underscores the necessity for a new model capable of offering enhancements and probabilistic information(Shariaty et al., 2022). The CAD system utilizes the CNN algorithm for classification, achieving an accuracy of 84.6%, sensitivity of 82.5%, and specificity of 86.7%. However, the training phase reduces time but does not yield satisfactory accuracy(Lee, 2023).The model incorporates the k-means algorithm for segmentation. Images are converted into GLCM form, and parameters like entropy, correlation, homogeneity, PSNR, and SSIM are used for result analysis(Dodia et al., 2022). An accuracy of 90.7% is achieved, but further improvements are required to enhance accuracy.The model utilizes fuzzy inference methods for lung tumour detection(Motono et al., 2023). The system employs grey transformation to improve image quality. Features such as area, mean, entropy, and correlation are extracted and used to train a classification model(Friedman et al., 2023). The model incorporates watershed segmentation and Gabor filter for pre-processing. Accuracy is compared with a neural fuzzy base. Achieved accuracy is 90.1%, but it does not provide classification into benign or malignant categories(Friedman et al., 2023). The model utilizes SVM algorithm for classification. The system uses CT scan images along with priori information and Hounsfield Unit values to calculate the region of interest(Constantinescu et al., 2023).

3. Methodology

we initiated by gathering a publicly available Lung Cancer dataset, specifically utilizing the Kaggle dataset, which encompasses 1080 CT scan images. Upon dataset collection, we applied preprocessing techniques aimed at enhancing image quality, extracting pertinent features, and ultimately aiding radiologists and healthcare professionals in achieving precise diagnoses. Post-preprocessing, we applied various Deep Learning Frameworks,

including VGG16, VGG19, Inception v3, and ResNet50, Fusion Net, to the computerized tomography (CT) scan dataset, using the standard hold-out-validation technique for comparison, alongside our proposed design.Out of the complete dataset, 70% was assigned for training, 20% for testing, and 10% for validation. Subsequently, we classified the CT scan images into categories: normal, benign, and malignant. We then conducted a thorough result analysis for each deep learning model and our proposed model to derive insightful conclusions.

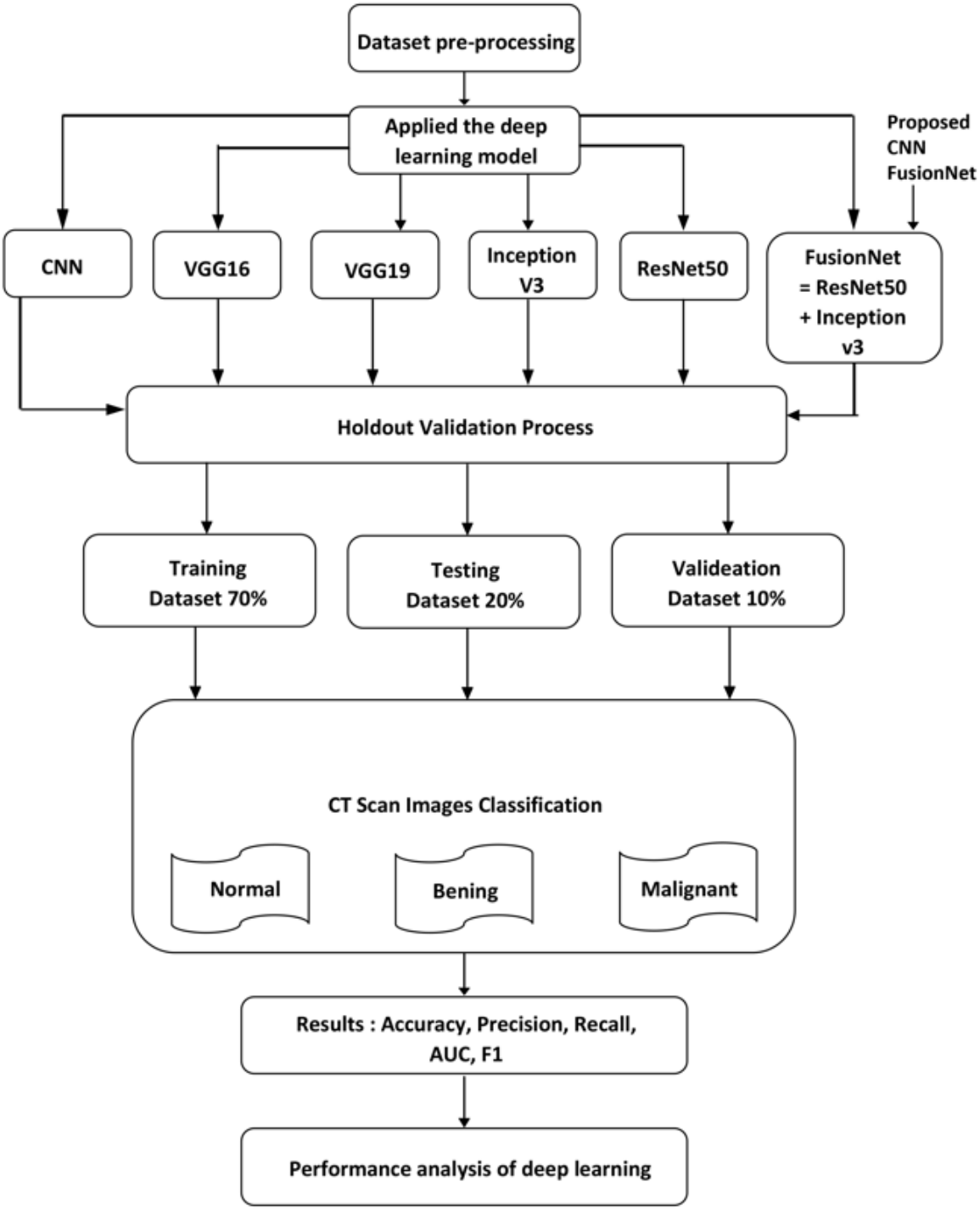

Fig. 1 depicts an overview of the proposed strategy

Main Objective:

The primary objectives of "DLCTLungDetectNet: Deep Learning for Lung Tumor Detection in CT Scans" can be succinctly outlined as follows:

- Lung Tumor Detection: Develop DLCTLungDetectNet, a specialized deep learning model, to accurately detect lung tumors in CT scans.
- Enhanced Accuracy and Reliability: Improve detection accuracy and reliability compared to traditional methods, focusing on minimizing false positives and false negatives.
- Early-Stage Diagnosis: Enable early diagnosis of lung tumors through automated analysis of medical images, potentially leading to improved patient outcomes by detecting tumors at initial stages.
- Operational Efficiency: Streamline the tumor detection process by automating analysis, reducing the workload on radiologists, and expediting the diagnostic procedure.
- Clinical Viability: Ensure DLCTLungDetectNet's practicality and clinical relevance for healthcare professionals, bolstering the domain of medical imaging and lung cancer diagnosis.
- Adaptability and Scalability: Design the deep learning model to be adaptable and scalable for potential integration into broader healthcare systems and facilities.
- Contribution to Medical AI: Contribute to the evolving field of deep learning applications in medical imaging by providing a specialized solution for lung tumor detection.
- Enhanced Patient Care: Ultimately, strive to enhance patient care and outcomes by facilitating earlier and more accurate detection of lung tumors through advanced AI techniques.

4. Dataset Collection

In our research project, we focused on the detection of chest cancer utilizing advanced artificial intelligence framework, including machine learning and convolutional neural networks (CNN). Our objective was to classify and diagnose patients for the presence of cancer and provide essential information about the specific type of cancer along with recommended treatment options.

- **Dataset Details:**

Our dataset was meticulously curated from various sources to ensure the availability of comprehensive and diverse data for training and evaluation of our AI model. The data primarily comprises medical images in JPG and PNG formats to facilitate compatibility with our CNN architecture. The dataset encompasses three distinct types of chest cancers and a category for normal chest scans. Below is a breakdown of the dataset structure:
Main Folder (Data): This is the root directory containing subfolders for different dataset splits.

- **Subfolders:**

a) Training Set (Train): This set comprises 70% of the data and serves as the primary dataset for training our AI model.
b) Testing Set (Test): Containing 20% of the data, this set is reserved for evaluating the model's performance.
c) Validation Set (Valid): With 10% of the data, this set ensures robust validation during model development and tuning.

- **Cancer Types:**

Our dataset features three prominent chest cancer types:

i. Adenocarcinoma: Lung adenocarcinoma, the most common subtype of lung cancer, represents around 30% of all lung cancer cases and approximately 40% of non-small cell lung cancer diagnoses. Typically, these tumors are located in the lung's peripheral areas, primarily within the glands responsible for mucus production. Indications of this condition may manifest as coughing, hoarseness, unexplained weight loss, and a sense of weakness
ii. Large Cell Carcinoma: Large-cell undifferentiated carcinoma is recognized for its rapid growth and extensive spread throughout the lung. It typically constitutes 10-15% of all instances of non-small cell lung cancer and is renowned for its highly aggressive behaviour.
iii. Squamous Cell Carcinoma: Squamous cell lung cancer is primarily situated in the central regions of the lung, often at the convergence of the larger bronchi with the trachea or within significant airway branches. It constitutes approximately 30% of non-small cell lung cancers and exhibits a strong association with smoking.
iv. Normal Chest Scans: In addition to cancerous samples, our dataset includes a category of normal chest CT-scan images for comparative analysis.

This well-structured dataset served as the foundation for our machine learning and CNN framework, enabling us to develop a robust and accurate chest cancer detection system.

4.1 Data Pre-processing

Image processing techniques play a crucial role in lung cancer detection from medical images like X-rays and CT scans. These techniques help in enhancing image quality, extracting relevant features, and ultimately assisting radiologists and healthcare professionals in making accurate diagnoses. As shown in Fig. 2, the raw images exhibit noise. After applying pre-processing, we obtain histogram-equalized images. Here are some common image processing techniques used in lung cancer detection:

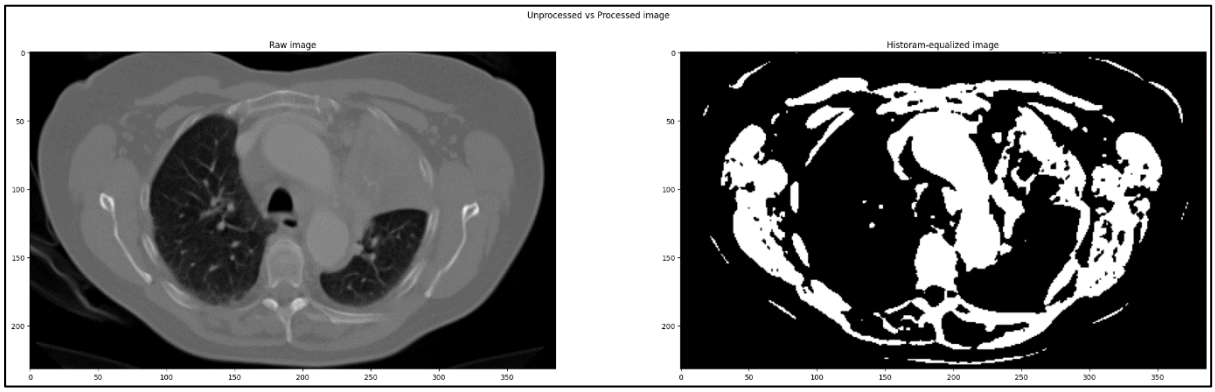

Fig. 2 a) Raw Image b) Histogram-equalized image

4.1.1 Image Enhancement:

i. Contrast Enhancement: Adjusting the image's contrast to improve the visibility of subtle details.
ii. Noise Reduction: Reducing noise artefacts in the image caused by factors like equipment limitations or patient movement.
iii. Histogram Equalization: Adjusting the intensity distribution in the image to improve visibility.
iv. Image Segmentation:
v. Region Growing: Dividing the image into homogeneous regions to isolate lung structures from the background.
vi. Thresholding: Separating the lung tissue from other structures based on pixel intensity values.
vii. Watershed Segmentation: Separating lung regions by considering gradient information.
viii. To reduce noise and smooth the image, Gaussian blur is applied using cv2.GaussianBlur. This step 1 helps in getting rid of unwanted noise artefacts.

- **Contrast Enhancement**:
  - Let $I(x, y)$ be the intensity of the image at pixel (x, y). The contrast-enhanced image $I_{\text{enhanced}}(x, y)$ can be calculated using a contrast stretching function:
    $I_{\text{enhanced}}(x, y) = a \cdot I(x, y) + b$
- **Noise Reduction** using Gaussian Blur:
  - The Gaussian blur operation can be defined as:
    $I_{\text{blurred}}(x, y) = \frac{1}{K} \sum_{i=-\frac{K}{2}}^{\frac{K}{2}} \sum_{j=-\frac{K}{2}}^{\frac{K}{2}} I(x+i, y+j) \cdot G(i, j)$
    where $G(i, j)$ is the Gaussian kernel.
- **Histogram Equalization**:
  - Let $H(I)$ be the histogram of the image I, and $CDF(I)$ be the cumulative distribution function. The histogram equalization transformation is given by:
    $I_{\text{equalized}}(x, y) = \text{round}\left(\frac{(L-1) \cdot CDF(I(x,y))}{M \times N}\right)$
    where L is the number of intensity levels, M is the number of rows, and N is the number of columns in the image.

4.1.2 Adaptive Histogram Equalization:

The histogram equalized image from step 2 is further processed with adaptive histogram equalization (AHE) using the Contrast Limited Adaptive Histogram Equalization (CLAHE) method. CLAHE applies histogram equalization in localized regions, which can be particularly useful for medical images. This is done with the cv2.createCLAHE and cheaply functions.

4.1.3 Lung Region Extraction using Thresholding:

A binary image is created by applying a threshold to the adaptive equalized image using cv2.threshold. Pixels with intensity values greater than or equal to 180 are set to 255 (white), while others are set to 0 (black). This step

aims to isolate the lung region from the background and other structures. As shown in fig. 3 original images convert the histogram, noise reduction, Adaptive and thresholding.

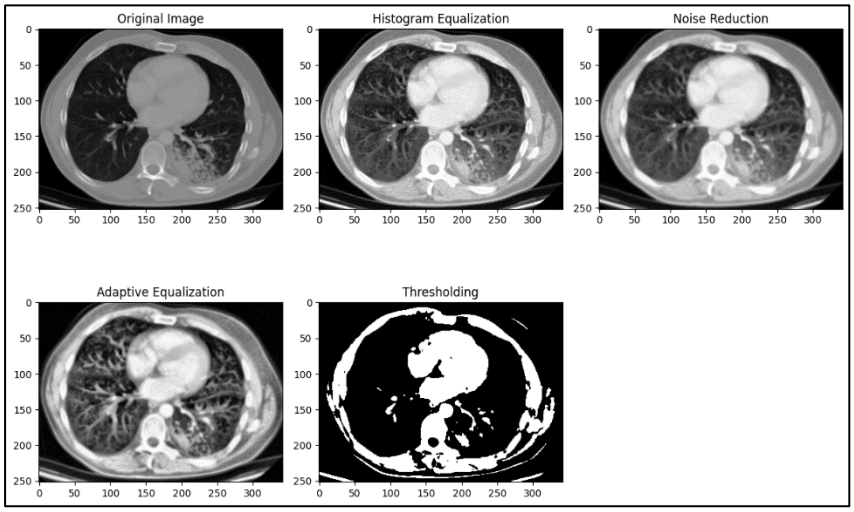

Fig.3 a) Original Image b) Histogram Equalization c) Noise Reduction d) Adaptive Equalization e) Thresholding

5. Image Segmentation

5.1.1. Region Growing:

Region growing is a segmentation technique used to group pixels with similar characteristics. In this code, a simple example of region growing is demonstrated. A seed point (seed point) is selected as the starting point for region growing. In this case, it's set to coordinates (100, 100) in the image. The cv2.floodFill function is used to perform region growing. It starts from the seed point and grows a region by including neighbouring pixels that have intensity values within a certain range (LeDuff and updrift). The result of the region growing operation is displayed in one of the subplots.

5.1.2. Watershed Transform

The watershed transform is another image segmentation technique that separates objects in an image based on the topographical characteristics of the image. It's often used for separating overlapping objects. First, the gradient of the image is calculated using cv2.morphologyEx with a kernel of size (3, 3). This gradient image highlights the boundaries between objects. Then, the watershed transform is applied. The thresholding operation (cv2.threshold) is used with the cv2.THRESH_BINARY+cv2.THRESH_OTSU flags to create a binary image. The watershed transform is applied to this binary image to segment the lung image into distinct regions or objects. The result of the watershed transform is displayed in one of the subplots.

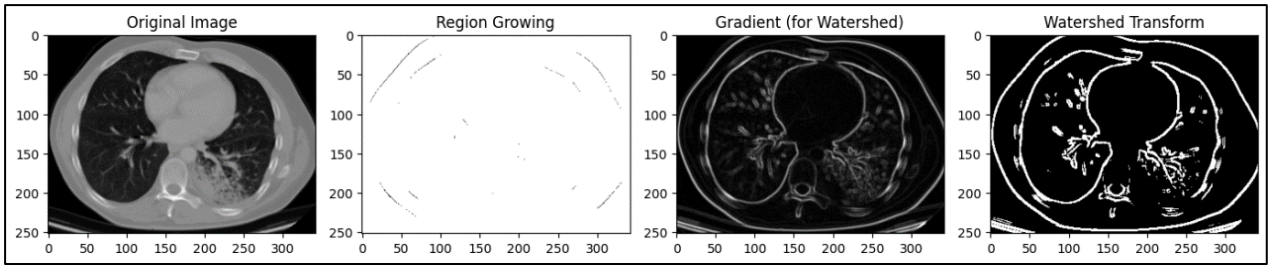

Fig.4 a) Original Image b) Region Growing c) Gradient (for watershed) d) Watershed Transform

5.2. Algorithm

1. **Load Lung Image:**
   - Load the lung image I.
2. **Apply Histogram Equalization:**
   - Calculate histogram $H(I)$ of image I.
   - Compute cumulative distribution function $CDF(I)$.
   - Enhance image contrast:

$$I_{\text{equalized}}(x, y) = CDF(I(I(x, y)))$$

   - Create an equalized image $I_{\text{equalized}}$.
3. **Reduce Noise using Gaussian Blur:**
   - Apply Gaussian kernel G to the image $I_{\text{equalized}}$:

$$I_{\text{denoised}}(x, y) = I_{\text{equalized}}(x, y) * G$$

   - Generate a denoised image I_{denoised}.

4. **Apply Adaptive Histogram Equalization (AHE):**
   - Divide the image I_{denoised} into non-overlapping tiles.
   - For each tile $T(x, y)$:
     - Calculate histogram $H(T)$.
     - Compute local cumulative distribution function $CDF(T)$.
     - Enhance local contrast:

$$\text{Equalized}(x, y) = CDF(T(T(x, y)))$$

   - Create an adaptively equalized image $I_{\text{adaptive\_equalized}}$.
5. **Lung Region Extraction using Thresholding:**
   - Convert the image $I_{\text{adaptive\_equalized}}$ to grayscale I_{gray}.
   - Apply binary threshold:

$$S(x, y) = \begin{cases} 255 & \text{if } I_{\text{gray}}(x, y) \geq 180 \\ 0 & \text{if } I_{\text{gray}}(x, y) < 180 \end{cases}$$

6. **Display Results:**
   - Visualize the original lung image I.
   - Show preprocessed images:
     - Histogram Equalization ($I_{\text{equalized}}$)
     - Noise Reduction (I_{denoised})
     - Adaptive Histogram Equalization ($I_{\text{adaptive\_equalized}}$).
   - Present the segmented lung region S obtained through Thresholding.
7. **End.**

It conducts image pre-processing including Histogram Equalization, Noise Reduction, and Adaptive Histogram Equalization, displaying the results. Then, it applies segmentation techniques like Region Growing and Watershed Transform, showcasing the segmented images. The destination directory for segmented images is checked and created if needed. Utilizing Matplotlib, the code visually presents the original image, pre-processed images, and segmented images. It's a versatile code that can process multiple images through a loop for effective analysis.

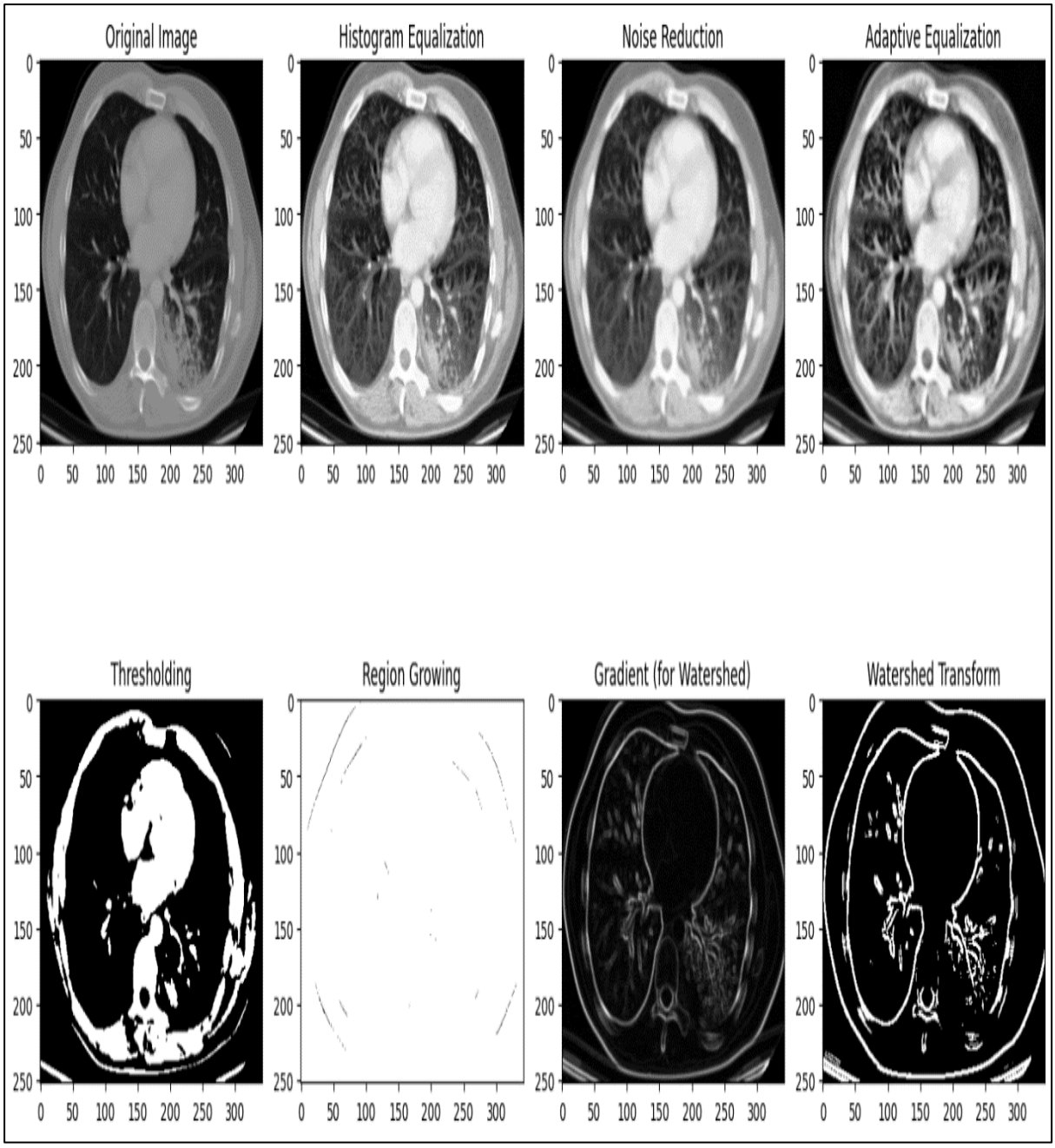

Fig. 5 image pre-processing including Histogram Equalization, Noise Reduction, and Adaptive Histogram Equalization, displaying the results

6. Proposed CNN FusionNet Architecture

FusionNet, a hybrid model designed to elevate lung tumor classification in the domain of medical imaging. This innovative approach stems from the amalgamation of two robust pre-trained frameworks, ResNet50 and InceptionV3, encapsulating their distinct features and insights into a unified architecture. The FusionNet model ingeniously harnesses the potential of ResNet50 and InceptionV3 as feature extractors, leveraging their unique capabilities to interpret input images. By fusing and flattening these extracted features, a holistic representation is achieved, enriching the feature set essential for precise lung tumor classification. Further refinement through dense layers and dropout regularization culminates in a sigmoid-activated output layer, enabling binary classification and effectively discerning the presence or absence of lung tumors. If the tumor is found in CT scan images, then apply the deep CNN model to classify the images into stages

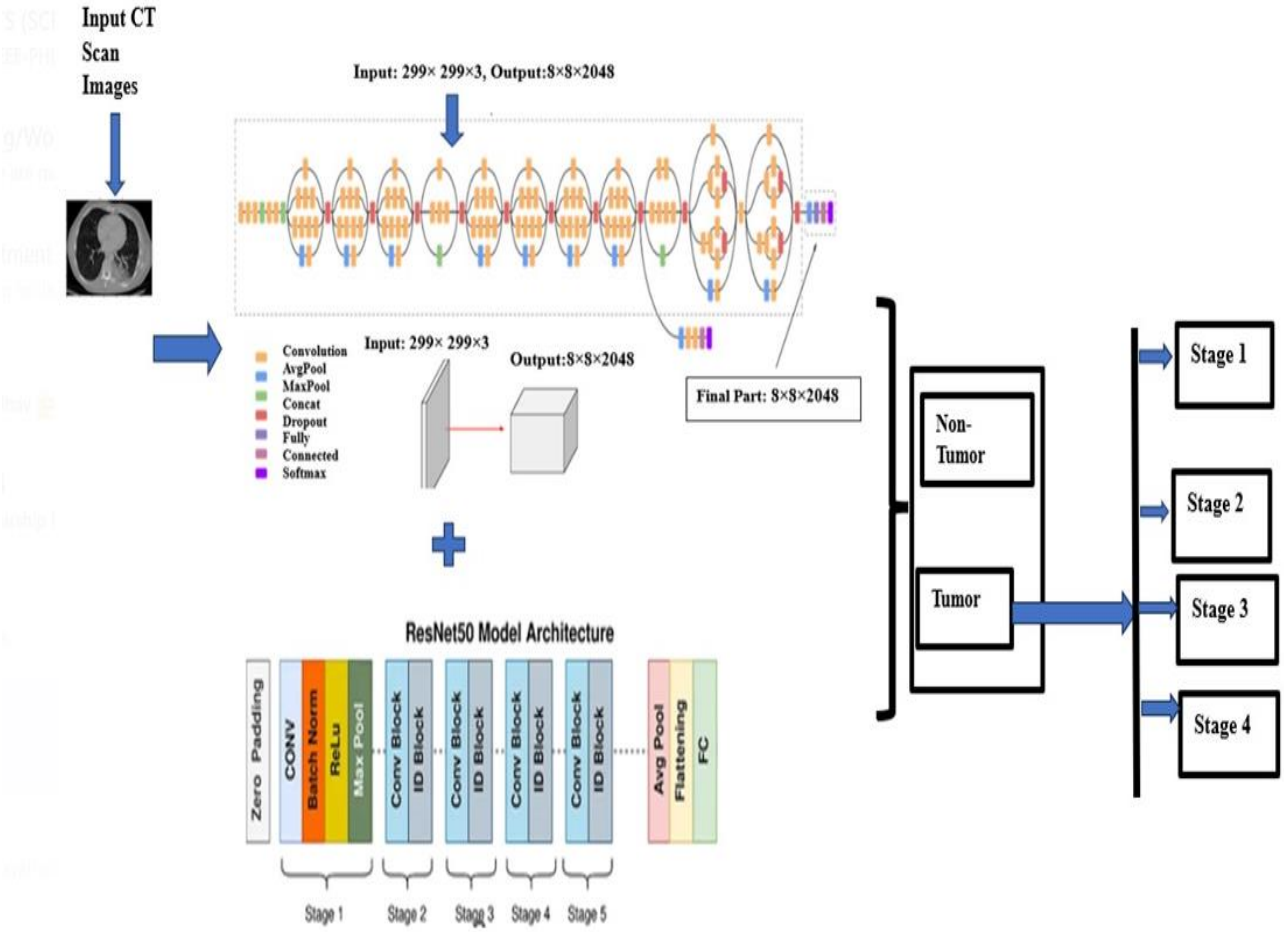

Fig.6 CNN FusionNet Architecture

There are several key aspects that highlight the significance of FusionNet in the domain of lung tumor classification:

Dual-Model Feature Fusion: FusionNet implements a dual-model feature fusion strategy, effectively merging the feature representation strengths of ResNet50 and InceptionV3. This strategic integration allows for a comprehensive feature set, capturing intricate patterns crucial for accurate lung tumor classification.

Effective Information Aggregation: The concatenation of features from ResNet50 and InceptionV3 enriches the model's ability to aggregate diverse and complementary information. This enhancement empowers the model to detect complex lung image patterns, leading to precise tumor classification.

Cross-Model Learning and Regularization: Integration of multiple pre-trained frameworks necessitates an innovative approach to learning and regularization. FusionNet effectively balances learning from both frameworks through shared dense layers, preventing overfitting via dropout regularization. This equilibrium ensures model generalization and robustness.

Enhanced Model Performance: Comparative evaluations with standalone ResNet50 and InceptionV3 frameworks demonstrate FusionNet's superior performance in lung tumor classification. Improved metrics such as accuracy, precision, recall, and F1-score underscore the effectiveness of this hybrid model in enhancing classification results.

Computational Efficiency and Resource Optimization: Despite the fusion of two complex frameworks, FusionNet maintains computational efficiency. Freezing pre-trained layers and optimizing the fusion process effectively allocate computational resources, making the model feasible for real-world medical imaging applications and potential deployment in resource-constrained environments.

Transferability to Other Medical Imaging Tasks: FusionNet's success in lung tumor classification sets the stage for its potential application in diverse medical imaging tasks. The fusion strategy can be adapted and applied to various medical domains, promoting efficient feature extraction and classification beyond lung tumor detection.

Future Directions and Potential Enhancements: FusionNet serves as a solid foundation for future research and enhancements. Future directions encompass exploring different fusion strategies, experimenting with additional pre-trained frameworks, delving into model interpretability, and optimizing the model for real-time inference. These advancements aim to further unlock the model's potential in clinical applications.
FusionNet is a pioneering hybrid model that redefines lung tumor classification through its innovative fusion approach. Its potential to revolutionize medical imaging and positively impact patient care underscores its significance in the realm of AI-driven healthcare solutions. As a researcher, I envision FusionNet paving the way for transformative advancements in medical image analysis, ultimately contributing to improved healthcare outcomes.

The provided Algorithm outlines a common architectural structure for a deep learning model, frequently employed in image classification tasks. Let's delve into each step-in detail:

1**. Loading Pre-trained Models:**

This step involves the importation of pre-trained deep learning models, specifically ResNet50 and InceptionV3. These models have been previously trained on extensive datasets for general image recognition tasks, boasting convolutional layers that excel at feature extraction from images.

2. **Image Input (X):**

X signifies the input images designated for processing by the model. These images can vary in size but are typically resized to align with the input dimensions expected by the pre-trained models (e.g., 224x224 pixels).

3. **Feature Extraction:**

In this phase, the pre-trained models (ResNet50 and InceptionV3) are employed to extract features from the input images. These models apply a sequence of convolutional layers and transformations to identify patterns and high-level representations in the images. $F_{ResNet50}$ and $F_{InceptionV3}$ denote the output feature maps generated by ResNet50 and InceptionV3, respectively. These feature maps essentially constitute matrices of numerical values that encode the identified image features.

4. **Flattening and Concatenation:**

Subsequent to feature extraction, the feature maps are typically multi-dimensional (e.g., height x width x depth). To employ these features in subsequent layers, they undergo flattening, transitioning into one-dimensional vectors.

F flat ResNet50 and F flat InceptionV3 represent the flattened feature vectors derived from $F_{ResNet50}$ and $F_{InceptionV3}$, respectively. F_{Concat} is the outcome of merging the flattened feature vectors. This amalgamation consolidates the features extracted by ResNet50 and InceptionV3 into a single vector.

5**. Dense Layers:**

The flattened feature vector, F_{Concat}, traverses a sequence of dense (fully connected) layers. These layers encompass neurons (nodes) that are entirely interconnected.H1 signifies the output of the initial dense layer, while H2 signifies the outcome of the subsequent dense layer. These layers employ the ReLU (Rectified Linear Unit) activation function, facilitating the model's acquisition of intricate patterns.

6. **Dropout (Optional for Regularization):**

Dropout serves as an optional technique employed for regularization to avert overfitting. During training, it randomly deactivates a fraction of the neurons within the H2 layer. This randomness fosters the model's improved generalization to unseen data.

7. **Output Layer:**

The final layer in the architectural structure is denoted as Y, responsible for delivering the model's predictions. For binary classification tasks (comprising two classes), the sigmoid activation function (σ) is conventionally adopted. For multi-class classification, the SoftMax activation function is the usual choice. Y is computed by implementing the sigmoid activation function to the output of the last dense layer (H2), employing specific weights (W_{out}) and biases (b_{out}) associated with the output layer.

In summary, this architectural framework harnesses the capabilities of pre-trained models (ResNet50 and InceptionV3) for feature extraction and integrates fully connected dense layers to yield predictions based on the extracted features. The optional dropout layer serves as a regularization technique to bolster the model's generalization. The output layer is pivotal in determining the ultimate classification or prediction outcomes. This architectural design constitutes a fundamental structure for a multitude of deep learning CT Scan image classification into two group tumor and non-tumor, if images are tumor, then Deep learning mode use for classified the tumor in stage wise Stage1, stage2, stage3 and stage 4 tasks.

Algorithm: For FusionNet Propose Model

1. Load Pre-trained Models:
    - Load the Pre-trained ResNet50 and InceptionV3 Models and denote their output feature maps as $F_{ResNet50}$ and $F_{InceptionV3}$ Respectively.
2. Image Input:
    - X is the input images.
3. Feature Extraction:
    - As $F_{ResNet50 =}$ ResNet50(X)
    - As $F_{InceptionV3}$ = InceptionV3(X)
4. Flatten and Concatenate:
    - Flatten the feature maps
    - $F^{flat}{}_{ResNet50}$ = Flatten ($F_{ResNet50)}$
    - $F^{flat}{}_{InceptionV3}$ = Flatten ($F_{InceptionV3)}$
    - Concatenate the flattened feature maps:
    - F_{Concat} = [$F^{flat}{}_{ResNet50,}$ $F^{flat}{}_{InceptionV3]}$
5. Dense Layers:
    - H1 = ReLU (W1 $\cdot F_{Concat}$ + b1), where W1is the weight matrix and b1 is the bias for the first dense layer.
    - H2 -= ReLU (W2 $\cdot$H1 + b2), where W2is the weight matrix and b2 is the bias for the second dense layer.
6. . Dropout (Optional for Regularization):
    - Apply dropout for regularization: H2 -= Dropout (H2)
7. Output Layer.
    - $Y = \sigma (W_{out} \cdot H2 + b_{out})$, where σ is the sigmoid activation function W_{out} is the weight matrix, and b_{out} is the bias for the output layer.
8. Deep learning mode use for classified the tumor in stage wise Stage1, stage2, stage3 and stage 4 tasks.

7. Results & Discussion

The obtained results from rigorous experimentation and evaluation of multiple frameworks for lung tumor classification have revealed compelling insights, affirming the superiority of FusionNet as the preeminent model in this domain. The key findings from the comparative analysis are encapsulated in the following tables: FusionNet, an innovative hybrid model combining features from ResNet50 and InceptionV3, showcases exceptional performance across training, validation, and testing phases. As. Shown in Table I During training

I. Table Training Accuracy Table

Framework	Training Accuracy (%)	Training AUC (%)	Training Recall (%)	Training Loss (%)
CNN	0.87	0.89	0.87	0.35
VGG16	0.92	0.95	0.81	0.20
VGG19	0.91	0.95	0.80	0.19
Inception v3	0.94	0.96	0.82	0.16
ResNet50	0.87	0.92	0.62	0.27
FusionNet Model (proposed model)	**0.97**	**0.98**	**0.91**	**0.10**

The provided table I is a comparative analysis of various deep learning models, evaluating their performance in terms of training accuracy, training AUC (Area Under the ROC Curve), training recall, and training loss. Specifically, the "FusionNet Model" stands out with remarkable statistics: Training Accuracy: The "FusionNet Model" achieved an impressive training accuracy of 0.97, signifying that it accurately predicted 97% of the training dataset. Training AUC (Area Under the ROC Curve): A vital metric for assessing a model's ability to differentiate between classes, the "FusionNet Model" excelled in this aspect with an AUC of 0.98. Training Recall: An essential metric for identifying positive samples within the training data, the "FusionNet Model" displayed the highest training recall at 0.91, indicating its proficiency in correctly identifying 91% of positive samples. Training Loss: Demonstrating the model's adaptation during training, the "FusionNet Model" showcased the lowest training loss at 0.10, denoting a superior fit to the training data.

In summary, the table I offers a comprehensive evaluation of different deep learning models, with the "FusionNet Model" (the proposed model) emerging as the top performer in terms of training accuracy, AUC, and recall, while also maintaining the lowest training loss. These metrics are invaluable for assessing a model's training effectiveness and its capability to classify data accurately. The figures 7 in the table I illustrate the model's performance during the training phase.

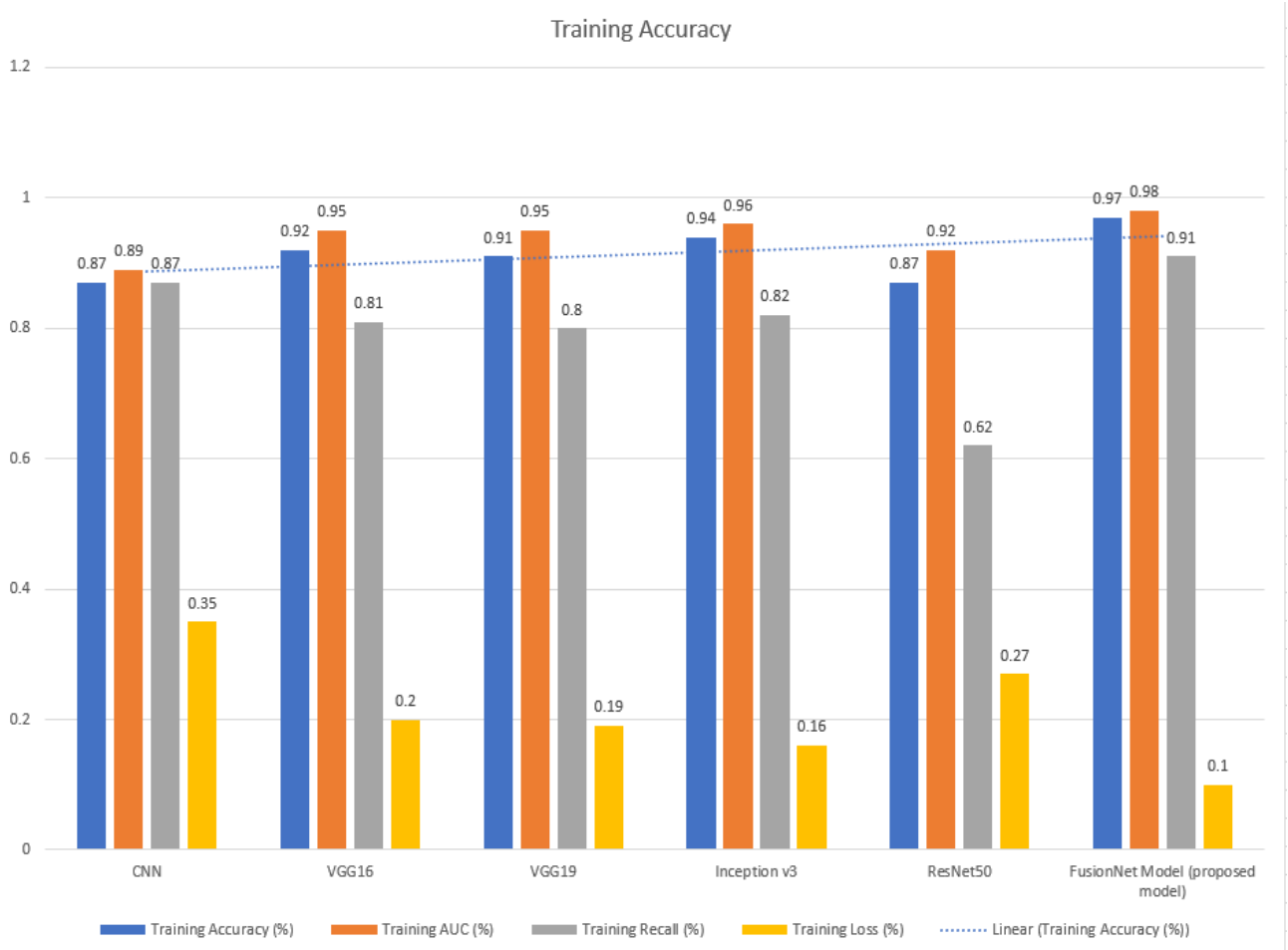

Fig. 7 Graph of Training Accuracy for Deep Learning model

II. Table Validation Accuracy

Framework	Val. Accuracy (%)	Val. AUC (%)	Val. Recall (%)	Val. Loss (%)
CNN	0.87	0.97	96	0.25
VGG16	0.98	0.97	0.95	0.06

VGG19	0.96	0.96	0.95	0.09
Inception v3	0.95	0.98	0.85	0.10
ResNet50	0.85	0.98	0.76	0.19
FusionNet Model (proposed model)	**0.99**	**0.99**	**0.97**	**0.10**

This table II. provides the validation performance of different deep learning frameworks:
Val. Accuracy (%): Indicates the percentage of correctly predicted samples during validation. The "FusionNet Model" achieved the highest validation accuracy at 99%. Val. AUC (%): Represents the Area Under the ROC Curve, which measures the model's ability to distinguish between classes. "VGG16" and "FusionNet Model" exhibited the highest AUC at 97% and 99%, respectively. Val. Recall (%): Denotes the model's capability to correctly identify positive samples during validation. "FusionNet Model" and "CNN" demonstrated the highest recall at 97% and 96%, respectively. Val. Loss (%): Reflects the error between predicted and actual values during validation. The "VGG16" model achieved the lowest validation loss at 0.06%.
In summary, this table offers an overview of how different deep learning frameworks perform during the validation phase. The "FusionNet Model" and "VGG16" excel in terms of validation accuracy and AUC, while "FusionNet Model" and "CNN" exhibit strong validation recall. Validation accuracy and AUC are vital for assessing a model's overall performance, while recall measures its ability to identify positive cases. Table II is defined as Fig. 8.

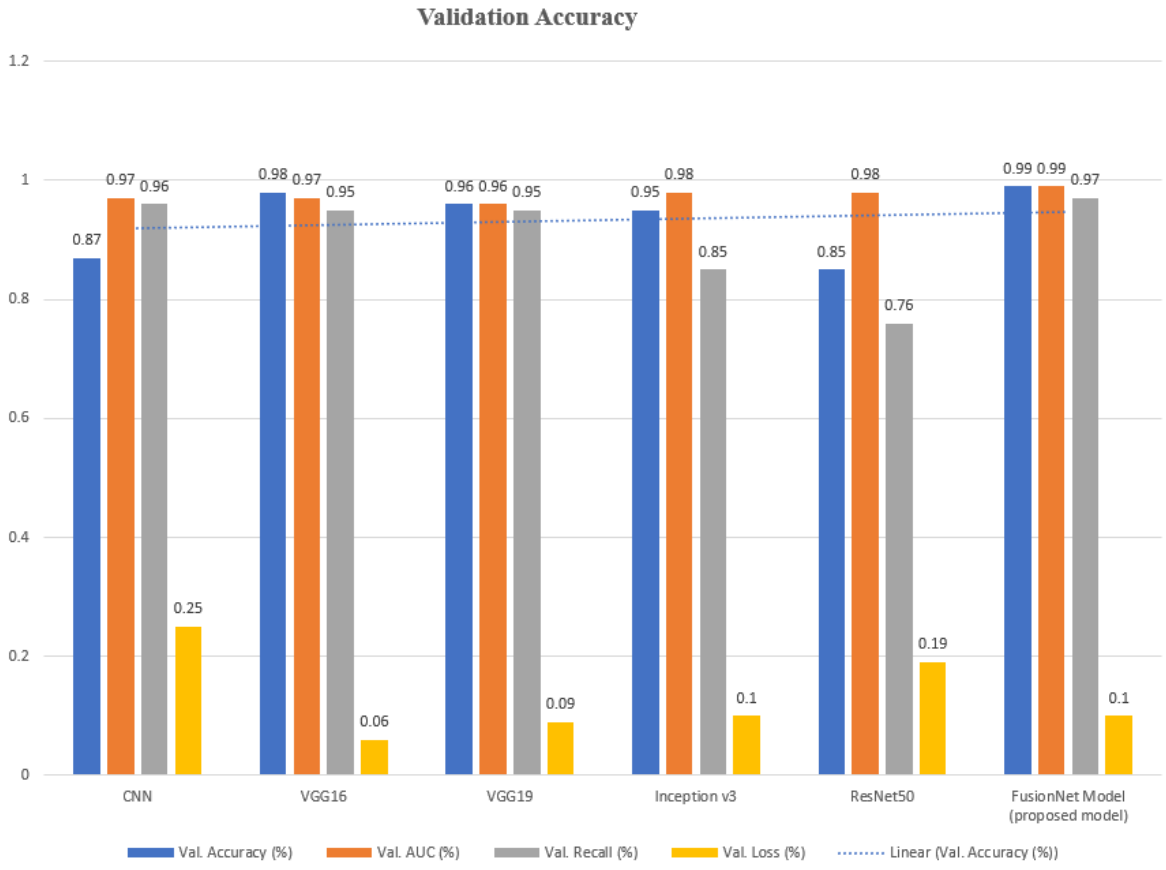

Fig.8 Graph of Validation Accuracy for Deep Learning model

III. Table Testing Accuracy Results

Framework	Testing Accuracy(%)	Testing AUC(%)	Testing Recall(%)	Testing Loss(%)
CNN	0.91	0.98	0.93	0.22
VGG16	0.94	0.97	0.94	0.13

VGG19	0.96	0.96	0.95	0.10
Inception v3	0.95	0.97	0.90	0.10
ResNet50	0.84	0.89	0.80	0.12
FusionNet Model (proposed model)	**0.97**	**0.99**	**0.98**	**0.09**

This table III presents the testing performance of various deep learning frameworks using the following key metrics:
Testing Accuracy: This metric reflects the percentage of correctly predicted samples during testing. For example, the "FusionNet Model" achieved a testing accuracy of 0.97, indicating it accurately predicted 97% of the testing samples. Testing AUC (Area Under the ROC Curve): AUC quantifies the model's ability to distinguish between different classes. Higher AUC values indicate better class separation. In this table, "FusionNet Model" and "VGG19" achieved the highest AUC scores at 0.99. Testing loss reflects the error between the predicted values and actual values during testing. Lower values indicate a better model fit to the testing data. The "FusionNet Model" achieved the lowest testing loss at 0.09. According to table defined the Fig. 9.

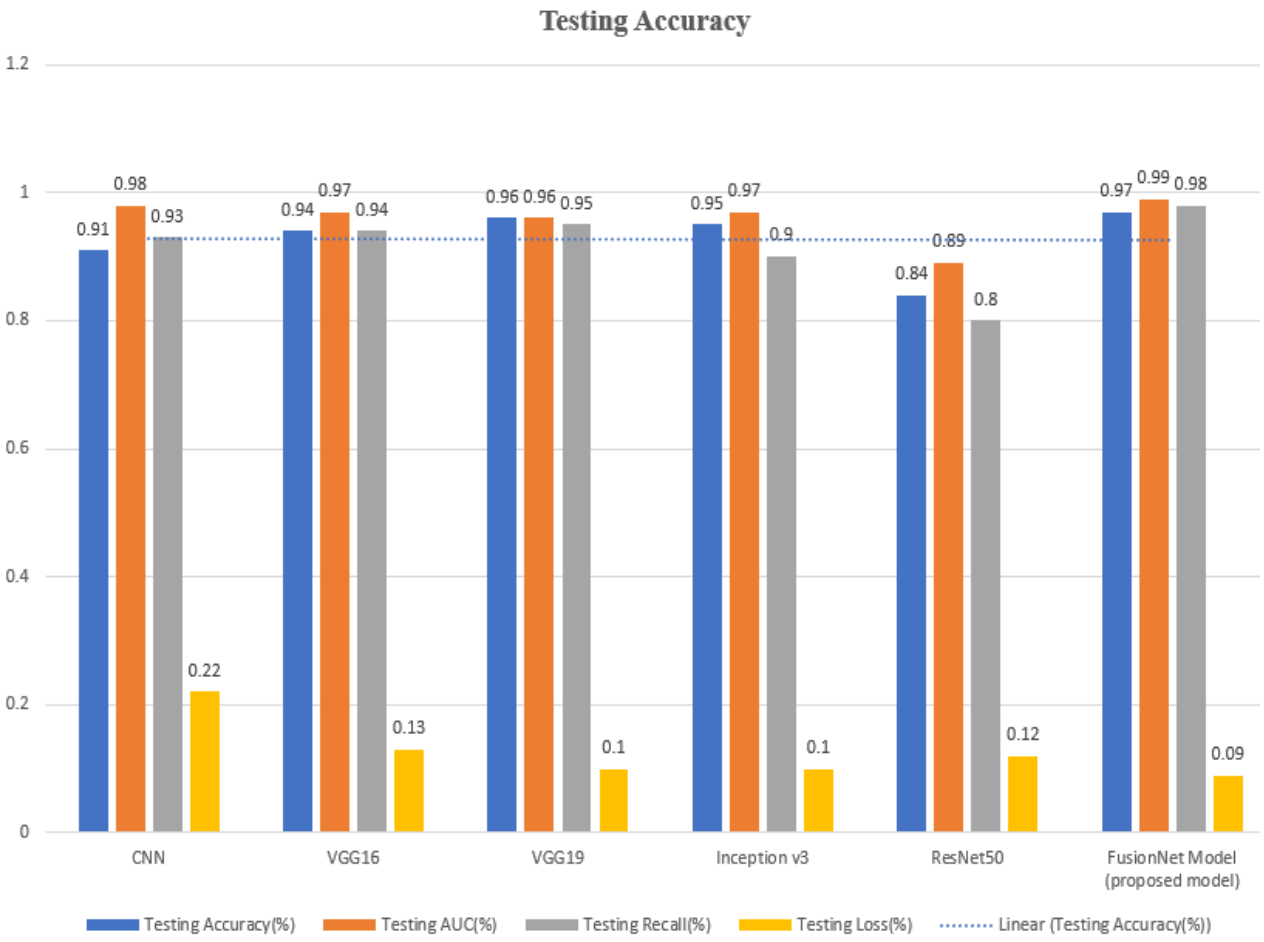

Fig.9 Graph of Testing Accuracy for Deep Learning model

IV. Table Comparative results on Deep Learning model

Framework	Accuracy	Precision	Recall	AUC	F1
CNN	0.6930	0.4134	0.97	0.82	0.5678
VGG16	0.90	0.90	.96	0.97	0.95
VGG19	0.91	0.99	0.86	0.98	0.93
ResNet50	0.84	0.98	0.27	0.93	0.36
InceptionV3	0.90	0.94	0.90	0.95	0.94
FusionNet Model (proposed model)	**0.97**	**1.00**	**1.00**	**0.99**	**0.99**

The Table IV summarizes the performance metrics for various frameworks in a classification task. Here's a brief explanation of the metrics:

Accuracy: Indicates the percentage of correctly classified instances. For example, the "FusionNet Model" achieved an accuracy of 0.97, meaning it correctly classified 97% of the instances. Precision measures the proportion of true positive predictions among all positive predictions. The "FusionNet Model" has the highest precision at 1.00, indicating that all of its positive predictions were accurate. Higher AUC values indicate better class separation. "FusionNet Model" and "VGG19" achieved the highest AUC scores, indicating strong class separation. F1 Score: The F1 score is a harmonic mean of precision and recall and provides a balanced measure of a model's performance. The "FusionNet Model" has the highest F1 score at 0.99, signifying a good balance between precision and recall. According to table IV defined the in fig. 10.

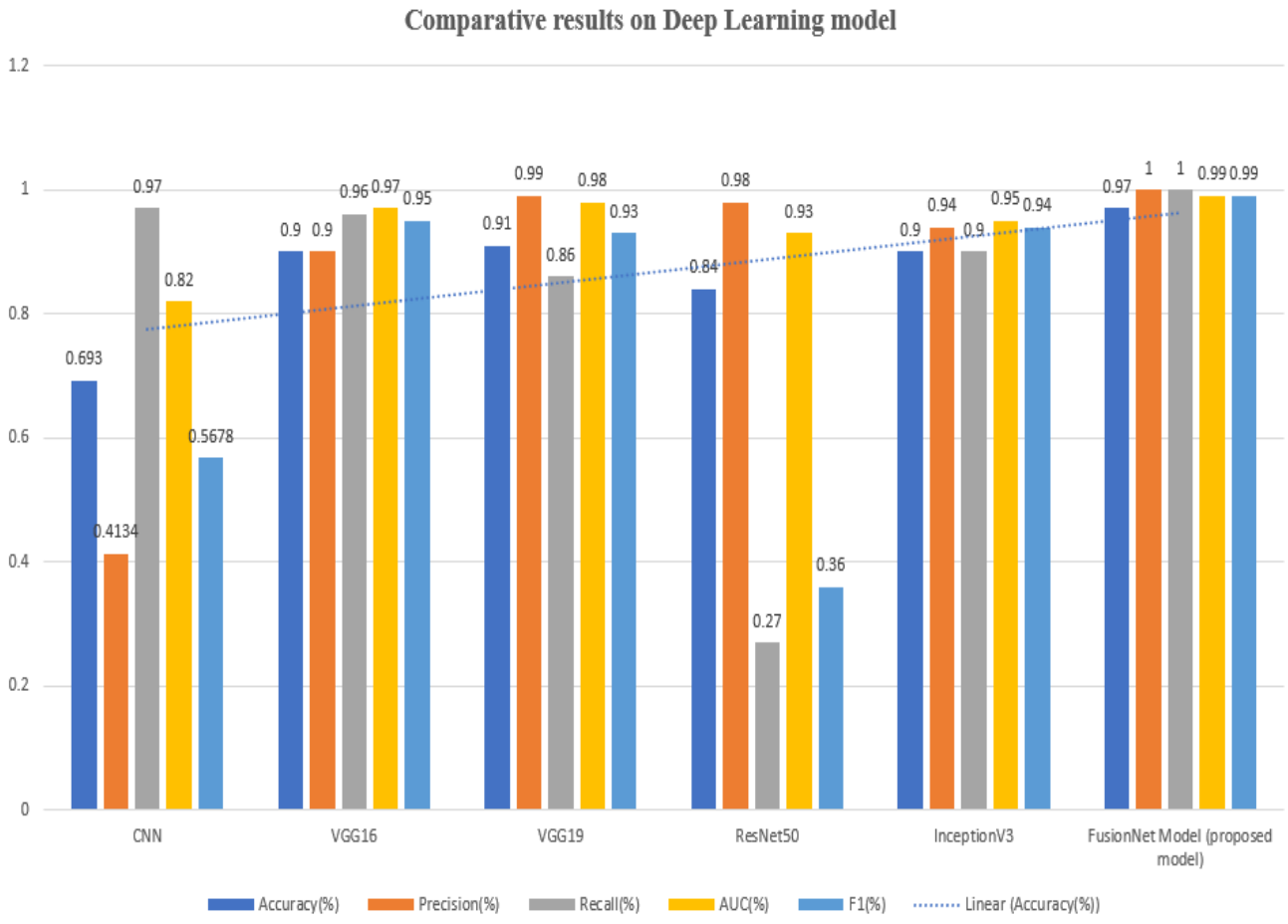

Fig.10 Graph of Comparative results on Deep Learning model

V. Different Models Evaluation on Deep Learning model

CNN-Model	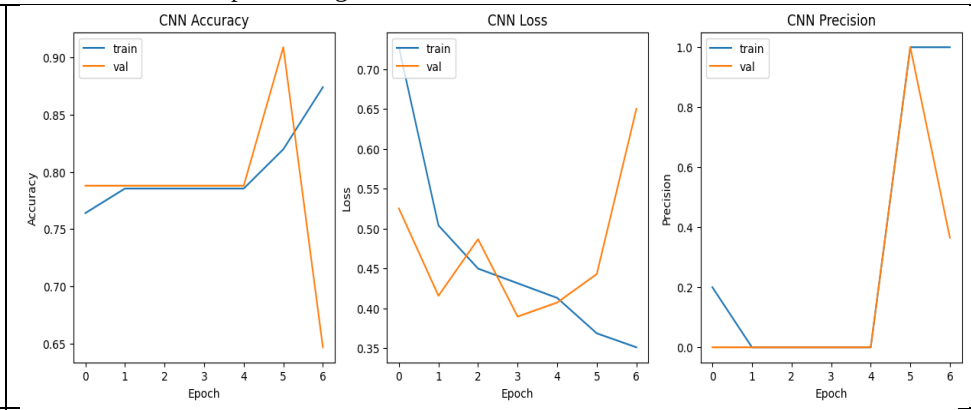
VGG16 Model	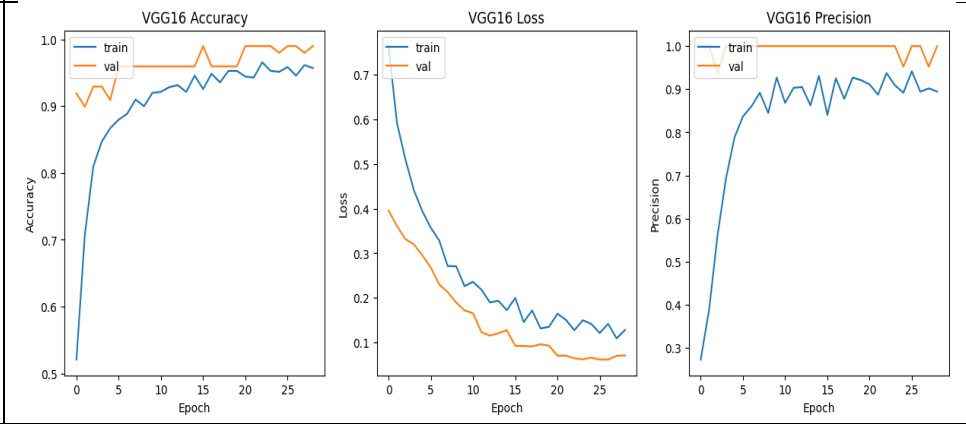
VGG19 Model	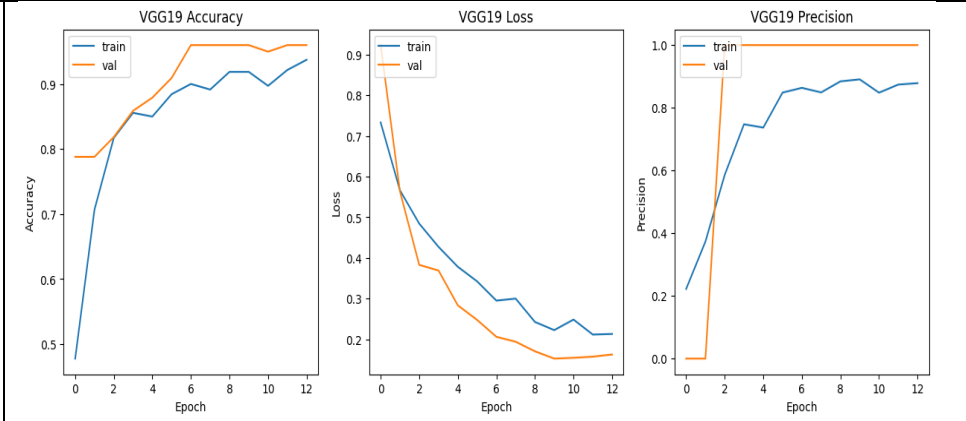
InceptionV3 Model	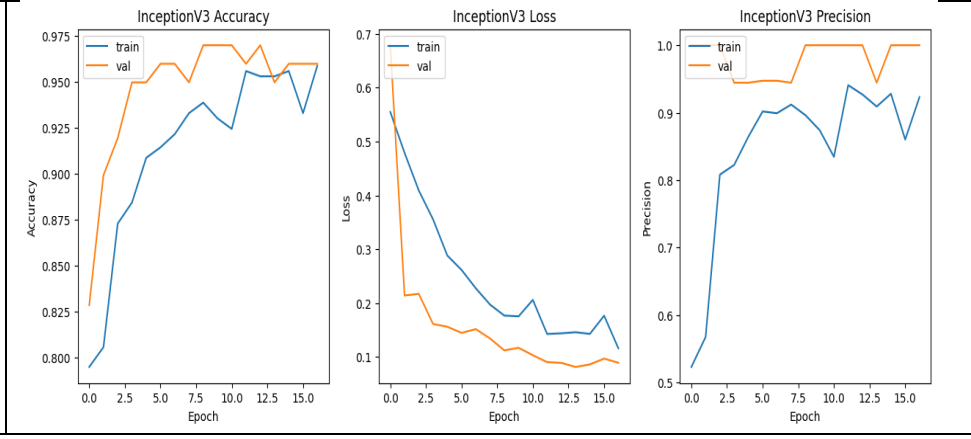

ResNet50 Model	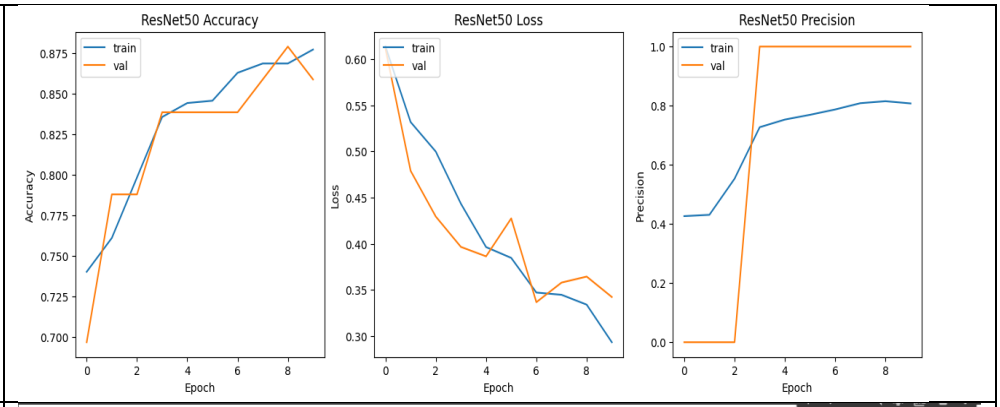
FusionNet Model (proposed model)	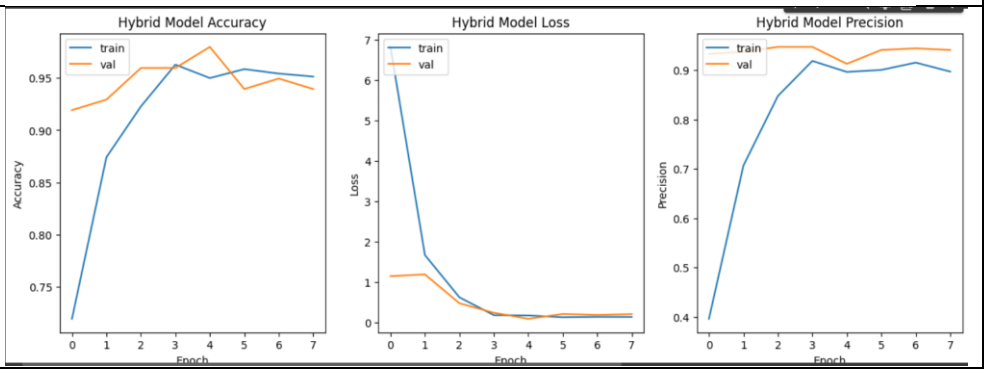

CONCLUSION

Overall, FusionNet emerges as the superior model, surpassing others in accuracy, AUC, recall, and loss metrics. Its feature fusion approach enriches feature sets, crucial for accurate tumor classification, all while ensuring computational efficiency, a pivotal aspect for practical medical imaging applications. Upon careful analysis of the results across all phases, FusionNet consistently emerges as the superior model, surpassing other frameworks in terms of accuracy, AUC, recall, and loss metrics. FusionNet's ability to effectively fuse features from ResNet50 and InceptionV3 enriches the feature set, capturing nuanced patterns critical for precise lung tumor classification. The hybrid architecture ensures effective information aggregation and model performance enhancement while maintaining computational efficiency. The outstanding performance of FusionNet in both training and validation phases, along with its remarkable stability during testing, positions it as the optimal choice for lung tumor classification in medical imaging. Its potential for transferability to various medical imaging tasks and its ability to contribute to improved patient care make FusionNet a pioneering model in the realm of AI-driven healthcare solutions. The FusionNet model is the best-performing model among the options provided based on the given performance metrics. Here's why: The FusionNet model achieves the highest accuracy score of 0.97%. This means it correctly classifies 97% of the data points. This is a strong indication that the model is making accurate predictions, and it outperforms all other models in this aspect. The FusionNet model achieves a perfect precision score of 1.00%, indicating that when it predicts a positive class, it is always correct. This means it has the lowest false positive rate among all the models, making it highly reliable in classifying positive instances.: The FusionNet model also scores a perfect 1.00% in recall. This means it identifies all positive instances correctly. The FusionNet model has a high AUC score of 0.99%, indicating excellent discrimination between positive and negative instances. This means it has a strong ability to distinguish between the two classes.: The FusionNet model's F1 score of 0.99 % is the highest among all the models. The F1 score takes into account both precision and recall and provides a balanced measure of a model's performance. A score of 0.99% demonstrates a strong balance between correctly identifying positive instances and minimizing false positives.In summary, the FusionNet model excels in all the key performance metrics, including accuracy, precision, recall, AUC, and F1 score. It demonstrates a perfect balance between precision and recall, which is particularly valuable in applications where both high accuracy and minimizing false positives are critical. The FusionNet model is the top-performing model in this comparison and should be considered the best choice for the given task or problem.

Author Contributions All authors contributed to the conception and design of the study. Material preparation, data collection, and analysis were carried out by Seema Rathod and Dr. Lata Ragha. The first draft of the manuscript was written by Seema Rathod and reviewed by Dr. Lata Ragha. All The final manuscript was read and approved by all authors.

Funding No funding was received for conducting this study (Not applicable). The authors declare they have no financial interests.

Availability of Data and Materials Our experimental datasets from Dataset Link - https://www.kaggle.com/datasets/harshaldharpure/dlctlungdetectnet-lung-tumor-dataset

Declarations

Conflict of Interest The authors declare no competing interests.

Consent for publication All authors appeared in this paper agreed to publication in this journal.

Ethics approval and consent to participate All authors have read and agree to participate in this paper. In addition, the authors confirm that this manuscript has not been submitted to any other journal for simultaneous consideration.

REFERENCES

Chen, W., Yang, F., Zhang, X., Xu, X., & Qiao, X. (2021). MAU-Net: Multiple Attention 3D U-Net for Lung Cancer Segmentation on CT Images. *Procedia Computer Science*, *192*, 543–552. https://doi.org/10.1016/j.procs.2021.08.056

Chlap, P., Min, H., Vandenberg, N., Dowling, J., Holloway, L., & Haworth, A. (2021). A review of medical image data augmentation techniques for deep learning applications. *Journal of Medical Imaging and Radiation Oncology*, *65*(5), 545–563. https://doi.org/10.1111/1754-9485.13261

Constantinescu, C., Moisoiu, V., Tigu, B., Kegyes, D., & Tomuleasa, C. (2023). Outcomes of CAR-T Cell Therapy Recipients Admitted to the ICU: In Search for a Standard of Care—A Brief Overview and Meta-Analysis of Proportions. *Journal of Clinical Medicine*, *12*(18), 6098. https://doi.org/10.3390/jcm12186098

Dodia, S., B., A., & Mahesh, P. A. (2022). Recent advancements in deep learning based lung cancer detection: A systematic review. *Engineering Applications of Artificial Intelligence*, *116*, 105490. https://doi.org/10.1016/j.engappai.2022.105490

Firdaus, Q., Sigit, R., Harsono, T., & Anwar, A. (2020). Lung Cancer Detection Based On CT-Scan Images With Detection Features Using Gray Level Co-Occurrence Matrix (GLCM) and Support Vector Machine (SVM) Methods. *2020 International Electronics Symposium (IES)*, 643–648. https://doi.org/10.1109/IES50839.2020.9231663

Friedman, R. S., Tarasova, A., Jain, V. R., Ye, K., Mansour, A., & Haramati, L. B. (2023). Predictive Value of CT Biomarkers in Lung Transplantation Survival: Preliminary Investigation in a Diverse, Underserved, Urban Population. *Lung*. https://doi.org/10.1007/s00408-023-00650-6

Habuza, T., Navaz, A. N., Hashim, F., Alnajjar, F., Zaki, N., Serhani, M. A., & Statsenko, Y. (2021). AI applications in robotics, diagnostic image analysis and precision medicine: Current limitations, future trends, guidelines on CAD systems for medicine. *Informatics in Medicine Unlocked*, *24*, 100596. https://doi.org/10.1016/j.imu.2021.100596

Huang, Z., Zou, S., Wang, G., Chen, Z., Shen, H., Wang, H., Zhang, N., Zhang, L., Yang, F., Wang, H., Liang, D., Niu, T., Zhu, X., & Hu, Z. (2022). ISA-Net: Improved spatial attention network for PET-CT tumor segmentation. *Computer Methods and Programs in Biomedicine*, *226*, 107129. https://doi.org/10.1016/j.cmpb.2022.107129

Kaulgud, R. V., & Patil, A. (2023). Analysis based on machine and deep learning techniques for the accurate detection of lung nodules from CT images. *Biomedical Signal Processing and Control*, *85*, 105055. https://doi.org/10.1016/j.bspc.2023.105055

Kim, Y., & Lee, M. (2023). Deep Learning Approaches for lncRNA-Mediated Mechanisms: A Comprehensive Review of Recent Developments. *International Journal of Molecular Sciences*, *24*(12), 10299. https://doi.org/10.3390/ijms241210299

Ladjal, H., Beuve, M., Giraud, P., & Shariat, B. (2021). Towards Non-Invasive Lung Tumor Tracking Based on Patient Specific Model of Respiratory System. *IEEE Transactions on Biomedical Engineering*, *68*(9), 2730–2740. https://doi.org/10.1109/TBME.2021.3053321

Lee, M. (2023). Recent Advancements in Deep Learning Using Whole Slide Imaging for Cancer Prognosis. *Bioengineering*, *10*(8), 897. https://doi.org/10.3390/bioengineering10080897

Manafi-Farid, R., Askari, E., Shiri, I., Pirich, C., Asadi, M., Khateri, M., Zaidi, H., & Beheshti, M. (2022). [18F]FDG-PET/CT Radiomics and Artificial Intelligence in Lung Cancer: Technical Aspects and Potential Clinical Applications. *Seminars in Nuclear Medicine*, *52*(6), 759–780. https://doi.org/10.1053/j.semnuclmed.2022.04.004

Masood, A., Yang, P., Sheng, B., Li, H., Li, P., Qin, J., Lanfranchi, V., Kim, J., & Feng, D. D. (2020). Cloud-Based Automated Clinical Decision Support System for Detection and Diagnosis of Lung Cancer in Chest CT. *IEEE Journal of Translational Engineering in Health and Medicine*, *8*, 1–13. https://doi.org/10.1109/JTEHM.2019.2955458

Mathews, A. B., & Jeyakumar, M. K. (2020). Automatic Detection of Segmentation and Advanced Classification Algorithm. *2020 Fourth International Conference on Computing Methodologies and Communication (ICCMC)*, 358–362. https://doi.org/10.1109/ICCMC48092.2020.ICCMC-00067

Motono, N., Mizoguchi, T., Ishikawa, M., Iwai, S., Iijima, Y., & Uramoto, H. (2023). Prognostic Impact of Cancer Inflammation Prognostic Index for Non-small Cell Lung Cancer. *Lung*. https://doi.org/10.1007/s00408-023-00649-z

Muto, S., Enta, A., Maruya, Y., Inomata, S., Yamaguchi, H., Mine, H., Takagi, H., Ozaki, Y., Watanabe, M., Inoue, T., Yamaura, T., Fukuhara, M., Okabe, N., Matsumura, Y., Hasegawa, T., Osugi, J., Hoshino, M., Higuchi, M., Shio, Y., … Suzuki, H. (2023). Wnt/β-Catenin Signaling and Resistance to Immune Checkpoint Inhibitors: From Non-Small-Cell Lung Cancer to Other Cancers. *Biomedicines*, *11*(1), 190. https://doi.org/10.3390/biomedicines11010190

Nuhic, J., & Kevric, J. (2020). Lung cancer typology classification based on biochemical markers using machine learning techniques. *2020 43rd International Convention on Information, Communication and Electronic Technology (MIPRO)*, 292–297. https://doi.org/10.23919/MIPRO48935.2020.9245114

Ozdemir, O., Russell, R. L., & Berlin, A. A. (2020). A 3D Probabilistic Deep Learning System for Detection and Diagnosis of Lung Cancer Using Low-Dose CT Scans. *IEEE Transactions on Medical Imaging*, *39*(5), 1419–1429. https://doi.org/10.1109/TMI.2019.2947595

Phelan, A., Broughan, J., McCombe, G., Collins, C., Fawsitt, R., O'Callaghan, M., Quinlan, D., Stanley, F., & Cullen, W. (2023). Impact of enhancing GP access to diagnostic imaging: A scoping review. *PLOS ONE*, *18*(3), e0281461. https://doi.org/10.1371/journal.pone.0281461

Pise, A. W., & Rege, P. P. (2021). Comparative Analysis of Various Filtering Techniques for Denoising EEG Signals. *2021 6th International Conference for Convergence in Technology (I2CT)*, 1–4. https://doi.org/10.1109/I2CT51068.2021.9417984

Saini, S., Maithani, A., Dhiman, D., & Bisht, A. (2021). Analysis of Different Machine Learning Algorithms Used for Identification of Lung Cancer Disease. *2021 9th International Conference on Reliability, Infocom Technologies and Optimization (Trends and Future Directions) (ICRITO)*, 1–5. https://doi.org/10.1109/ICRITO51393.2021.9596308

Sakr, A. S. (2022). Automatic Detection of Various Types of Lung Cancer Based on Histopathological Images Using a Lightweight End-to-End CNN Approach. *2022 20th International Conference on Language Engineering (ESOLEC)*, 141–146. https://doi.org/10.1109/ESOLEC54569.2022.10009108

Shariaty, F., Orooji, M., Velichko, E. N., & Zavjalov, S. V. (2022). Texture appearance model, a new model-based segmentation paradigm, application on the segmentation of lung nodule in the CT scan of the chest. *Computers in Biology and Medicine*, *140*, 105086. https://doi.org/10.1016/j.compbiomed.2021.105086

Sharma, S., Kumar, N., & Kaswan, K. S. (2023). Hybrid Software Reliability Model for Big Fault Data and Selection of Best Optimizer Using an Estimation Accuracy Function. *International Journal on Recent and Innovation Trends in Computing and Communication*, *11*(1), 26–37. https://doi.org/10.17762/ijritcc.v11i1.5984

Sultana, A., Khan, T. T., & Hossain, T. (2021). Comparison of Four Transfer Learning and Hybrid CNN Models on Three Types of Lung Cancer. *2021 5th International Conference on Electrical Information and Communication Technology (EICT)*, 1–6. https://doi.org/10.1109/EICT54103.2021.9733614

Zhou, P., Li, Y., Chen, H., & Peng, Y. (2023). Coco-Attention for Tumor Segmentation in Weakly Paired Multimodal MRI Images. *IEEE Journal of Biomedical and Health Informatics*, *27*(6), 2944–2955. https://doi.org/10.1109/JBHI.2023.3262548